RSC Advances

PAPER

View Article Online
View Journal | View Issue

Cite this: *RSC Adv.*, 2020, **10**, 36526

Catalytic/magnetic assemblies of rolled-up tubular nanomembrane-based micromotors†

Sumayyah Naeem,‡[ab] Jawayria Mujtaba,‡[b] Farah Naeem,[ab] Kailiang Xu,[c] Gaoshan Huang,[b] Alexander A. Solovev,*[b] Jing Zhang*[d] and Yongfeng Mei[b]

Nano/-micromotors self-assembling into static and dynamic clusters are of considerable promise to study smart, interactive, responsive, and adaptive nano/-micromaterials that can mimic spatio-temporal patterns, swarming, and collective behaviors widely observed in nature. Previously, the dynamic self-assembly of bubble-propelled catalytic micromotors initiated by capillary forces has been reported. This manuscript shows novel self-assembly modes of magnetic/catalytic Ti/FeNi/Pt tubular micromotors. When chemical fuel (hydrogen peroxide) is added it is decomposed on contact with Pt catalyst into oxygen and water. Here, the non-bubbling motion and autonomous assembly of catalytic/magnetic nanomembranes, *i.e.* without nucleation/generation of oxygen bubbles, are shown. Moreover, magnetic Ti/FeNi/Pt micromotors are spun using an external magnetic field and they form dynamic clusters balanced by attractive magnetic and repulsive hydrodynamic interactions. Micromotors form dynamic clusters, undergo precession and rapidly propagate through the solution.

Received 27th August 2020
Accepted 21st September 2020

DOI: 10.1039/d0ra07347d

rsc.li/rsc-advances

1. Introduction

Recently, considerable literature has grown up around the theme of micromotors prepared for cross-disciplinary research and diverse applications.[1–3] Inspired by the small size of nature's machines, working uninterruptedly and smoothly to sustain and support life,[2] micromotors with different shapes (rod, tube, sphere, *etc.*), size, material combinations, fuel composition and methods of control have been demonstrated.[4] The self-propelled motion of the micromotors is achieved by self-electrophoresis, self-diffusiophoresis, and bubble recoil.[5] Versatile methods to control directionality, speed and power of micromotors have been developed using external fields (*e.g.*, magnetic field, light, electrochemical potential and ultrasound).[6] In this current world, where natural resources are running out and microbial viruses are causing havoc, designing efficient man-made nano/-and micromachines is a step forward towards the realization of biomedical,[7,8] environmental[9,10] and clean energy tasks.[11]

Experimental test-bed systems enabled by micromotors have attracted a high interest to explore emergent collective, swarming behaviours and more complex nano/-micromachines based on self-assembly systems.[12–14] One of the interesting pertaining features – chemical reactions and motive forces of nano/-micromotors can be used to modify well-known static interactions among micro/-nanomachines.[15] Moreover, external fields can be employed to effectively control the dynamic self-assembly of active particles. For example, hydrophobic–hydrophilic interactions have been used to assemble millimetre-scale boats self-propelled by the decomposition of hydrogen peroxide.[1] A long-range capillary interaction has been used to achieve a swarming behaviour of microbubble-propelled catalytic tubes.[16] In the latter case, ejected oxygen microbubbles during the decomposition of hydrogen peroxide change the curvature of the air–liquid interface, leading to competing capillary and motive forces of tubular micromotors.[17] When the bubble size decreases the capillary force reduces and the swarming micromotors self-disassemble or spread. Another notable example shows light-illuminated particles that release ions with different diffusion coefficients, leading to the appearance of an electric field. Autonomous microparticles respond to the electric field and they can attract or repel each other depending on their charges. Ag_3PO_4 micromotors driven by self-diffusiophoresis have shown collective behaviours in water by the reversible non-redox reaction, *i.e.* a shift in chemical equilibrium influenced by NH_3 or UV light.[18] Much attention has been attracted by the study of assemblies of micromotors and their interactions powered by light that influences photo-thermal effects, photo-chemical reactions, optical forces and photoisomerizations.[19] Photo-responsive assemblies of "living crystals" consisted of colloidal particles

[a]*State Key Laboratory for Modification of Chemical Fibers, Polymer Material Science and Engineering, Donghua University, Shanghai 201620, China*
[b]*Department of Materials Science, Fudan University, Shanghai 200433, China. E-mail: solovevlab@gmail.com*
[c]*Department of Electronic Engineering, Fudan University, Shanghai 200433, China*
[d]*College of Science, Donghua University, Shanghai 201620, China*

† Electronic supplementary information (ESI) available. See DOI: 10.1039/d0ra07347d

‡ These authors contributed equally.

have been driven by competing motive and phoretic/osmotic effects.[20] Light-powered AgCl micromotors self-propel by self-diffusiophoresis, release ions, interact and self-assemble into "schools".[21] Another study shows spatio-temporal patterns of Ag-based motors, controlled by the periodical "on and off" illumination with multiple observed dynamic behaviours controlled by frequencies of light switching.[22] Recently, it has been reported that a short-range attractive interaction can appear from electrical forces during oxidation–reduction reactions.[23] Another approach shows an application of the rotational magnetic field to assemble dynamic spinners made of millimetre-sized magnetic disks, which are attracted to the axis of magnetic field rotation and repelled from each other by the spinning hydrodynamic force.[24] Non-equilibrium patterns can also arise in non-biological electrochemical molecular systems, such as Turing-like patterns, self-organized on the surface of the electrode.[25]

In this study, novel assembly modes of magnetic/catalytic Ti/FeNi/Pt nanomembrane-based tubular micromotors are reported. Magnetic, catalytic, hydrodynamic and electro-kinetic effects-driven interactions potentially responsible for self-assembly behaviours are discussed in detail. When hydrogen peroxide fuel is added to the solution containing microtubes, they convert hydrogen peroxide fuel into oxygen and water. Threshold concentrations of hydrogen peroxide are identified, which lead to the formation of microbubbles (*i.e.*, "active" microtubes). It is known that bubbles lead to capillary interactions of tubular micromotors at the air–liquid interface. Here, non-bubbling motion and assembly of catalytic nanomembranes are studied in solutions containing hydrogen peroxide. In the presence of the permanent magnetic field, Ti/FeNi/Pt micromotors change their direction and align themselves according to the direction of the magnetic field. Subsequently, magnetic Ti/FeNi/Pt microtubes are spun using an external magnetic field, leading to the formation of dynamic interactive clusters and spinning vortexes.

2. Experimental section

Rolled-up catalytic micromotors made of strain-engineered nanomembranes are fabricated using the rolled-up nanotechnology method discussed elsewhere.[16] Ti/FeNi/Pt microtubes are produced by electron beam (e-beam) evaporation of thin metallic films on square photoresist patterns. AR-P 3510 photoresist is spin-coated on a silicon 1.5-inch wafer at 3500 rpm for 35 s, followed by soft baking at 90 C for 2 min. Then, the patterns are exposed to the UV light using Karl Suss MA-56 mask aligner for 7 s. Photoresist patterns are developed in the 1 : 1 AR300-35/H_2O solution. On-chip rolled-up catalytic microtubes with layers thicknesses 10/10/5 nm (detected by the quartz crystal, oriented perpendicularly to the beam). Materials are deposited on samples at the tilted angle 60° (measured from the horizontal axis). Angular deposition method helps to get microtubes integration on the sample surface. The pre-stressed multilayers are self-rolled-up into microtubes by dissolving the sacrificial photoresist layer in the acetone solvent. A supercritical point dryer is used to dry the microtubes without collapsing. Optical microscopy images are captured using the Olympus optical microscope and videos are recorded using a high-speed camera at 190 frames per s. An external NdFeB magnet is used to produce a 3 mT magnetic field around the sample for magnetic alignment of tubes. Magnetic stirring plate was used to create rotational magnetic field with microtubes located in the Petri dish on the surface of stirring plate.

3. Results and discussions

Swarming and collective behaviours of micromotors can be achieved using external fields and catalytic reactions. Fig. 1(a and b) displays schematic and optical microscopy images of fabricated rolled-up microtubes. Fig. 1(c) shows a basic principle of the dynamic self-assembly of two microtubes based on competing motive and capillary interactions. In the latter case, the capillary attraction is the result of ejected microbubbles from micromotors at the air–liquid interface.[16,17] Fig. 1(d) indicates a schematic image of magnetic microtubes rotated using an external rotational magnetic field. Spinning micromotors attract each other by the magnetic and simultaneously repel by the hydrodynamic motion of a fluid. Fig. 2(e) shows magnetic self-assembly of microtubes after they are magnetized. Fig. 1(e) illustrates a schematic image of the electro-kinetic effects-driven self-assembly of tubes during the oxidation–reduction reactions of catalytic thin films. Here, micromotors bind by the opposite oxidation and reduction parts.

In this study, the term "nanomembrane" is used to describe a freestanding thin film with a thickness below 100 nm and

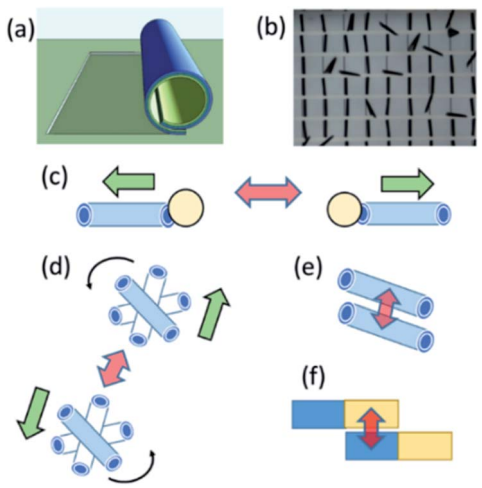

Fig. 1 Fabrication and basic principles of magnetic/catalytic assemblies of rolled-up tubular nanomembrane-based micromotors. (a) A schematic image of the rolled-up microtube fabricated using the under-etching of the sacrificial layer. (b) Optical microscopy image of microtube arrays with tube length 50 μm. (c) Competing attractive capillary (red arrow) and repulsive motive (green arrow) interactions between bubble-propelled micromotors. (d) Rotation of magnetic microtubes leading to a magnetic attraction and hydrodynamic repulsion between two motors. (e) An assembly of magnetic tubes using a static external magnetic field. (f) Electro-kinetic effects-driven attraction of microtubes during the oxidation–reduction reaction of thin catalytic films.

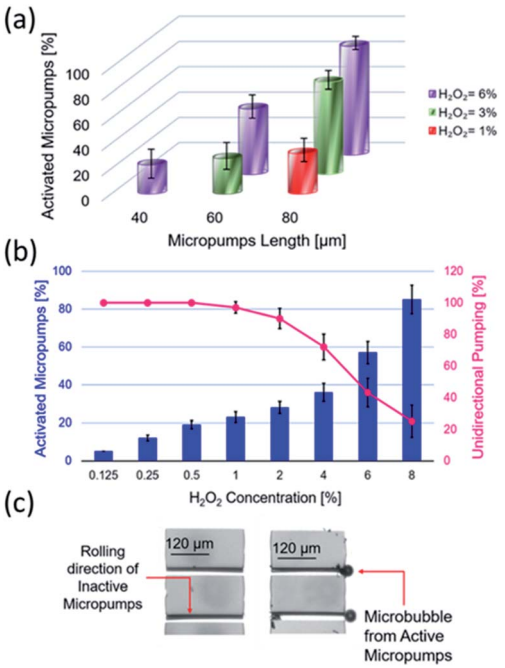

Fig. 2 Characterization of Ti/FeNi/Pt microtubes in a hydrogen peroxide solution. (a) Population of active microtubes (generating O_2 bubbles) with lengths 40, 60 and 80 μm immersed in H_2O_2 1% v/v (red colour), 3% v/v (green colour), and 6% v/v (purple colour), respectively. (b) The population of activated microtubes with 120 μm length. Percentages of active microtubes with 120 μm length in unidirectional (bubbles' ejection from one tubular opening) and overloaded (bubbles' ejection from both tubular openings) regimes. (c) Optical microscopy image of inactive microtubes (*i.e.*, generating molecular oxygen, O_2 microbubbles are absent) and active tubes (*i.e.*, producing visible O_2 microbubbles).

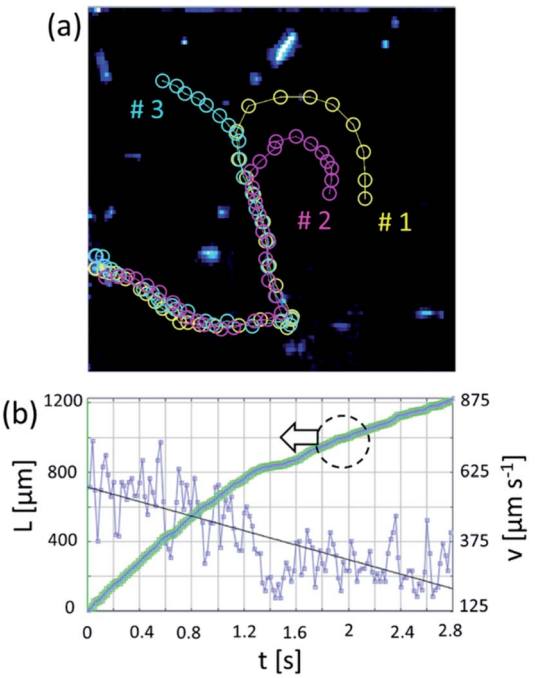

Fig. 3 Motion without oxygen bubbles and self-assembly of Ti/FeNi/Pt microtubes in the mixture of propylene carbonate and hydrogen peroxide solution. (a) Tracked trajectories of motion of three individual micromotors. (b) Analysis of travelled distance and tracked velocity of #1 micromotor during 2.8 s. A linear fit shows the decrease in speed after the collective binding of several micromotors into a larger moving cluster.

a large aspect ratio. Rolled-up nanomembranes form microtubes, which operate as catalytic microreactors or micromotors during decomposition of hydrogen peroxide into oxygen and water. Microtubes generate oxygen microbubbles more efficiently than planar catalytic layers due to the confinement of molecular oxygen in reaction and diffusion processes. So far, motion and assembly of catalytic nanomembrane-based tubular micromotors in the non-bubbling regime have not yet been explored. Previously, it was determined that the tubular aspect ratio is a crucial parameter for both activations of tubes in unidirectional (*i.e.*, ejection of O_2 bubbles) and overloaded regimes (generation of bubbles from both tubular openings).[26–28] Fig. 2(a) shows the population of activated Ti/FeNi/Pt microtubes with lengths 40, 60 and 80 μm immersed in 1, 3 and 6 v/v % H_2O_2, respectively. At 1% v/v H_2O_2: 32.5% of 80 μm long tubes are activated. While at H_2O_2 3% v/v: 28% of 60 μm and 73% v/v of 80 μm long tubes are activated. At 6% v/v H_2O_2: 23% of 40 μm long tubes start generating O_2 bubbles, 52% of the 60 μm and 86% v/v of the 80 μm long tubes are activated. These results were previously explained by molecular diffusion of molecular oxygen over the length of tube: nucleation of bubbles require a supersaturating of gaseous molecules. Longer tubes confine longer diffusive molecular oxygen, leading to a gas supersaturation and an appearance of favourable conditions for bubbles' generation.[4] For self-assembly, it is essential to examine conditions for bubbling and non-bubbling regimes. Fig. 2(b) shows the dependence of hydrogen peroxide concentration on the population of activated microtubes and unidirectional bubble recoil for 120 μm long tubes. Fig. 2(c) shows an optical micrograph of inactive (*i.e.* molecular oxygen diffuses without the formation of bubbles) and active (bubbles are generated) microtubes.

Non-bubbling conditions can be used to explore novel self-assembly modes of catalytic nanomembranes previously reported. In hydrogen peroxide and propylene carbonate mixture tubular catalytic micromotors are capable to self-propel without bubbles. Fig. 3(a) shows motion and assembly of Ti/FeNi/Pt rolled-up nanomembranes in the solution of propylene carbonate with added hydrogen peroxide (2% v/v). As expected (from Fig. 2) bubbles do not nucleate for shorter microtubes and some fraction of longer microtubes remain without O_2 bubbles. Fig. 3(b) shows tracked trajectories of motion and assembly of Ti/FeNi/Pt nanomembrane-based micromotors. Micromotors #1 self-propel at an average speed 480 μm s^{-1}. Propelling nanomembranes self-assemble by the magnetic interaction and form larger moving clusters. After binding, micromotor #1 decreases its average speed to 340 μm s^{-1}. Moreover, the magnetic field can be used to induce static and dynamic assemblies of nanomembrane-based tubular micromotors. Fig. 4(a) shows a schematic of the magnetic assembly of Ti/FeNi/Pt microtubes in the propylene carbonate solvent.

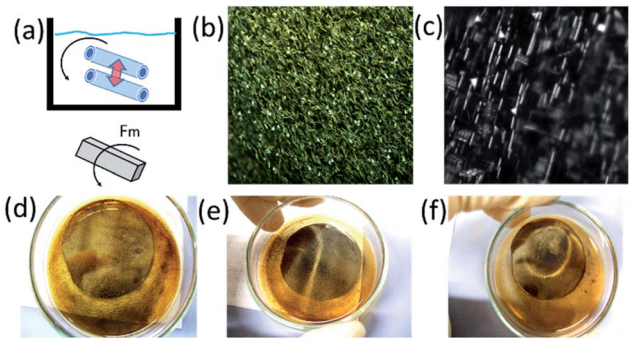

Fig. 4 An assembly of microtubes in solutions using an external magnetic field. (a) Schematic image of magnetic alignment of Ti/FeNi/Pt tubes. (b) Non-magnetized microtubes have random orientations in solutions. (c) Magnetized microtubes align and self-assemble along the long axis of tubular symmetry. (d) Scratched arrays of microtubes in the solution of propylene carbonate (without magnetic field). (e) A magnet bar is placed underneath the Petri dish to assemble tubes into a linear pattern. (f) The formation of a circular pattern consisted of microtubes by changing the position of the magnet.

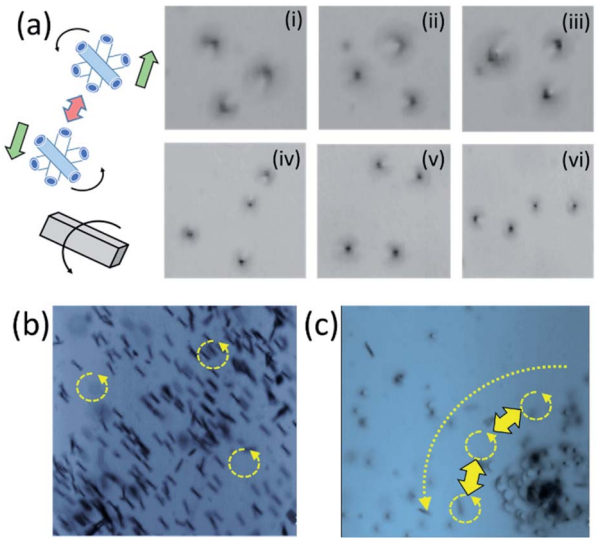

Fig. 5 The dynamic self-assembly of tubular magnetic micromotors with length 50 μm using a rotational magnetic field. (a) Schematic image of magnetic tubular nanomembranes that spin and form spatio-temporal assemblies by using magnetic–hydrodynamic interactions. (i–iii) Three spinners form a stable dynamic cluster. (iv–vi) Four spinners assemble into the dynamic cluster that rapidly changes its configuration. (b) Rotation of magnetic microtubes using a rotational magnetic field (stirring plate) at 100 rpm (optical micrograph). Circular arrows show the direction of rotation. (c) Rotation of Ti/FeNi/Pt microtubes at 1000 rpm and observation of vortexes (optical micrograph). Double arrows show hydrodynamic–magnetic interactions among microtubes. A large circular arrow indicates the direction of vortex rotation, where individual microtubes rotate and precess around the vortex centre.

Fig. 4(b) demonstrates a large number of released tubes in solution. Fig. 4(c) demonstrates an influence of the external magnetic field and a subsequent tubes self-alignment in the magnetic field. Fig. 4(d–f) are optical camera images of linear and circular patterns controlled using magnet positioned underneath the Petri dish (not shown). Patterns are visible because multiple tubes reflect white light in one direction. After the magnet is removed the patterns are "self-erased" due to the tubes' alignment in random directions.

Spatio-temporal assemblies of particles can be formed in a solution using a rotational magnetic field and hydrodynamic interactions.[24] Tubes (Ti/FeNi/Pt) containing a magnetic layer spin around their axis, self-propel towards the centre of the magnetic field and repel from each other by fluid motion around the solid–liquid boundaries. Rolled-up magnetic Ti/FeNi/Pt microtubes are rotated using an external magnetic field (solution with tubes are placed on a stirring plate, not shown). Fig. 5(a(i–iii)) demonstrates the formation of a dynamic cluster consisted of three interacting micromotors (ESI Video 1†). The cluster rapidly precesses in time without changing its configuration. However, when the four's micromotor is added, shown in Fig. 5(a(iv–vi)), the cluster loses its stability and micromotors' evolve into different dynamic configurations (ESI Video 2†). If longer tubes are added into the solution, it creates larger vortexes, due to larger inertial effects of the fluid. Subsequently, smaller spinners precess around the larger spinners, while the centre of such vortexes propagates towards the centre of stirring plate, *i.e.* the centre of the rotational magnetic field. At a low frequency of magnetic field (100 rpm), microtubes do not interact (Fig. 5(b), ESI Video 3†), while at a higher rotational speed (1000 rpm) interactions start (Fig. 5(c), ESI Video 4†). The Reynolds number can be estimated for the dynamic micromotors: $\mathrm{Re} = \rho\omega a^2/\mu$, where ω is the typical rotation speed of spinner, ρ is the fluid density, a is the motor radii and μ is the shear viscosity.[24] The theory predicts that stable dynamic patterns should form for $\mathrm{Re} \sim 1$. We assume that for the tubular length (spinner diameter) 50 μm in the propylene carbonate solvent the Reynolds number is slightly larger since the micromotors are undergoing precession.

4. Conclusions

This study shows the dynamic self-assembly of nanomembrane-based catalytic/magnetic Ti/FeNi/Pt tubular micromotors. Micromotors self-propel by decomposition of hydrogen peroxide into oxygen and water. Bubbles' nucleation/generation depends on the concentration of hydrogen peroxide fuel and the tube aspect ratio (diameter/length). For the first time, non-bubbling tubes are explored and it is shown that catalytic Ti/FeNi/Pt microtubes are capable to self-propel without the formation of oxygen bubbles in the mixture of hydrogen peroxide and propylene carbonate. Since the discovery of nanorod-based nanomotors[2,3] the issue of nanomotors' motion mechanism (bubble recoil, self-electrophoresis, self-diffusiophoresis) has been a controversial and much-disputed subject. The previously unexplored motion of catalytic nanomembrane-based micromotors without bubbles, *i.e.* using phoretic effects, can be of significant importance for the design of smaller scale catalytic nanomotors. During motion, micromotors self-assemble into larger clusters. Here, we accept that magnetic interaction is responsible for nanomembranes

assemblies. Further study is required to elucidate the detailed mechanism of propulsion and assembly of non-bubbling catalytic nanomembrane-based tubular micromotors. For instance, previously it was reported that catalytic non-magnetic nanorods can bind to each other by electro-kinetic effects originated from the oxidation–reduction reactions.[23] Moreover, we demonstrate that magnetic Ti/FeNi/Pt tubes can be used as micromotors forming dynamic clusters balanced by magnetic attraction and hydrodynamic repulsion. Micromotors spin around their axis, precess and create vortexes in the propylene carbonate solvent. In the future, it is of high interest to understand how different tubular lengths influence the formation of vortexes. These results, inspired by the collective behaviour in nature, tend to demonstrate principles of smart micromachines towards the construction of adaptive, responsive and interaction nanomaterials, capable to change configurations of individual dynamic components by chemical reactions and external fields.

Conflicts of interest

There are no conflicts to declare.

Acknowledgements

The authors thank the financial support from the National Natural Science Foundation of China grants (No. 51602056, 51961145108, U1632115, 51475093), Science and Technology Commission of Shanghai Municipality (17JC1401700), the National Key Technologies R&D Program of China (2015ZX02102-003), the Program of Shanghai Academic Research Leader (19XD1400600), BRICS Foundation and the Changjiang Young Scholars Program of China.

Notes and references

1 R. F. Ismagilov, A. Schwartz, N. Bowden and G. M. Whitesides, *Angew. Chem., Int. Ed.*, 2002, **41**, 652.
2 G. A. Ozin, I. Manners, S. Fournier-Bidoz and A. Arsenault, *Adv. Mater.*, 2005, **17**, 3011.
3 W. F. Paxton, K. C. Kistler, C. C. Olmeda, A. Sen, S. K. St. Angelo, Y. Cao, T. E. Mallouk, P. E. Lammert and V. H. Crespi, *J. Am. Chem. Soc.*, 2004, **41**, 13424.
4 H. Ning, Y. Zhang, H. Zhu, A. Ingham, G. Huang, Y. F. Mei and A. A. Solovev, *Micromachines*, 2018, **9**, 75.
5 J. Wang, *Nanomachines: Fundamentals and Applications*, WILEY-VCH, 2013, ISBN: 978-3-527-33120-8.
6 Q. L. Yang, L. Xu, W. Zhong, Q. Yan, Y. Gao, W. Hong, Y. She and G. Yang, *Advanced Intelligent Systems*, 2020, 2000049.
7 L. Sonntag, J. Simmchen and V. Magdanz, *Molecules*, 2019, **24**, 3410.
8 X. Lin, B. Xu, H. Zhu, J. Liu, A. A. Solovev and Y. F. Mei, *Research*, 2020, **2020**, 1.
9 J. G. S. Moo and M. Pumera, *Chem.–Eur. J.*, 2015, **21**, 58.
10 J. Liu, H. Chen, X. Shi, S. Nawar, J. G. Werner, G. Huang, M. Ye and D. A. Weitz, *Environ. Sci.: Nano*, 2020, **7**, 656.
11 V. V. Singh, F. Soto, K. Kaufmann and J. Wang, *Angew. Chem., Int. Ed.*, 2015, **127**, 7000.
12 C. Liu, T. Xu, L. P. Xu and X. Zhang, *Micromachines*, 2018, **9**, 10.
13 B. A. Grzybowski, K. Fitzner, J. Paczesny and S. Granick, *Chem. Soc. Rev.*, 2017, **46**, 5647.
14 L. L. A. Adams, D. Lee, Y. F. Mei, D. A. Weitz and A. A. Solovev, *Adv. Mater. Interfaces*, 2020, **7**, 1901583.
15 C. Wang, Q. L. Wang, R.-F. Dong and Y.-P. Cai, *Inorg. Chem. Commun.*, 2018, **91**, 8.
16 A. A. Solovev, Y. F. Mei and O. G. Schmidt, *Adv. Mater.*, 2010, **22**, 4340.
17 A. A. Solovev, S. Sanchez and O. G. Schmidt, *Nanoscale*, 2013, **5**, 1284.
18 W. Duan, R. Liu and A. Sen, *J. Am. Chem. Soc.*, 2013, **135**, 1280.
19 J. Zhang, J. Guo, F. Mou and J. Guan, *Micromachines*, 2018, **9**, 88.
20 J. Palacci, S. Sacanna, A. P. Steinberg, D. J. Pine and P. M. Chaikin, *Science*, 2013, **339**, 936.
21 M. Ibele, T. E. Mallouk and A. Sen, *Angew. Chem., Int. Ed.*, 2009, **48**, 3308.
22 X. Chen, C. Zhou, Y. Peng, Q. Wang and W. Wang, *ACS Appl. Mater. Interfaces*, 2020, **12**, 11843.
23 W. Wang, W. Duan, A. Sen and T. E. Mallouk, *Proc. Natl. Acad. Sci. U. S. A.*, 2013, **110**, 17744.
24 B. A. Grzybowski, H. A. Stone and G. M. Whitesides, *Nature*, 2000, **405**, 1033.
25 Y.-J. Li, J. Oslonovitch, N. Mazouz, F. Plenge and K. Krischer, *Science*, 2001, **291**, 2395.
26 S. Naeem, F. Naeem, J. Zhang, J. Mujtaba, K. Xu, G. Huang, A. A. Solovev and Y. F. Mei, *Micromachines*, 2020, **11**, 643.
27 S. Naeem, F. Naeem, J. Liu, V. A. B. Quiñones, J. Zhang, L. He, G. Huang, A. A. Solovev and Y. F. Mei, *Chem.–Asian J.*, 2019, **14**, 2431–2434.
28 S. Naeem, F. Naeem, M. Manjare, F. Liao, V. A. Bolaños Quiñones, G. S. Huang, A. A. Solovev and Y. F. Mei, *Appl. Phys. Lett.*, 2019, **114**, 033701.

